CAIT-UTC-NC60

Development and Validation of Methodologies for Rapid Inspection and Assessment of Fatigue Damage

FINAL REPORT
September 2020

Submitted by:
Sougata Roy, Ph.D., Associate Research
Professor Department of Civil and Environmental Engineering
Center for Advanced Infrastructure and Transportation
Rutgers, the State University of New Jersey
100 Brett Road
Piscataway, 08854

External Project Manager
Jean H. Laird, P.E., Senior Project Engineer
New Jersey Turnpike Authority (NJTA)
1 Turnpike Plaza
Woodbridge, NJ 07095

In cooperation with

Rutgers, The State University of New Jersey
And
New Jersey Turnpike Authority (NJTA)
And
U.S. Department of Transportation
Federal Highway Administration

Disclaimer Statement

The contents of this report reflect the views of the authors, who are responsible for the facts and the accuracy of the information presented herein. This document is disseminated under the sponsorship of the Department of Transportation, University Transportation Centers Program, in the interest of information exchange. The U.S. Government assumes no liability for the contents or use thereof.

The Center for Advanced Infrastructure and Transportation (CAIT) is a National UTC Consortium led by Rutgers, The State University. Members of the consortium are the University of Delaware, Utah State University, Columbia University, New Jersey Institute of Technology, Princeton University, University of Texas at El Paso, Virginia Polytechnic Institute, and University of South Florida. The Center is funded by the U.S. Department of Transportation.

TECHNICAL REPORT STANDARD TITLE PAGE

1. Report No.	2.Government Accession No.	3. Recipient's Catalog No.
CAIT-UTC-NC60		

4. Title and Subtitle	5. Report Date
Development and Validation of Methodologies for Rapid Inspection and Assessment of Fatigue Damage	September, 2020
	6. Performing Organization Code CAIT/Rutgers University
7. Author(s) Sougata Roy, Ph.D.	8. Performing Organization Report No. CAIT-UTC-NC60
9. Performing Organization Name and Address Center for Advanced Infrastructure and Transportation Rutgers, The State University of New Jersey 100 Brett Road, Piscataway, NJ 08854	10. Work Unit No.
	11. Contract or Grant No. DTRT13-G-UTC28
12. Sponsoring Agency Name and Address Center for Advanced Infrastructure and Transportation Rutgers, The State University of New Jersey 100 Brett Road Piscataway, NJ 08854	13. Type of Report and Period Covered Final Report 09/01/2018- 12/31/2019
	14. Sponsoring Agency Code

15. Supplementary Notes
U.S. Department of Transportation/OST-R
1200 New Jersey Avenue, SE
Washington, DC 20590-0001

16. Abstract

Causes of unusual fatigue cracking of a steel bridge owned by the New Jersey Turnpike Authority (NJTA) was investigated by Finite Element Analysis (FEA). The bridge is located on a strategic commerce route and is subjected to high Average Daily Truck Traffic (ADTT) consisting of significant fraction of overloaded trucks having Gross Vehicle Weight as high as twice the legal limit. The bridge originally built in 1950s and widened in 1971 is in service for more than 60 years. Fatigue cracking was observed in the top flange of the floor beams at deck expansion joints. The cracks developed at bearing stiffeners under the stringers and grew through the flange at some locations. Based on Weigh-in-Motion (WIM) studies performed at a nearby bridge, the bridge model was analyzed for 2.25 times the AASHTO fatigue design truck load plus 15% impact. The analysis showed that the maximum stress in the floor beam flange developed when the rear tandem axle of the truck loading crossed over to the deck on one side of the expansion joint. The maximum stress range occurred under the loaded bearing on the floor beam bracket, which was remnant from the original construction and was incorporated into the deck widening. The fatigue cracking in the flange adjacent to the bearing stiffeners was due to cyclic plastic straining. The local stresses at the holes for the bearing retaining bolts also exceed the yield limit of the material leading to fatigue cracks in the flange emanating from the holes. Due to significantly larger section modulus of the interior floor beam, the stresses in the flange was less than the AASHTO CAFT for Category A or base metal. No fatigue crack growth was observed nor was expected at this location. The analysis showed that the fatigue cracking was due to frequently occurring overloaded trucks in the truck traffic spectrum. The fatigue cracking was expected to be localized under the widened section of the bridge carrying the two exterior lanes mostly traversed by truck traffic, where the section modulus of the floor beam was significant less than that of the floor beams between the interior girders. Based on the findings, it is recommended that the exterior floor beam between the exterior and the first interior girder be strengthened to reduce the stresses in the flange below the CAFT of respective details.

17. Key Words	18. Distribution Statement
Fatigue Cracking, Floor beam, Compression Flange, Steel Bridges, Fatigue Retrofit	

19. Security Classif (of this report)	20. Security Classif. (of this page)	21. No of Pages	22. Price
Unclassified	Unclassified	38	

Form DOT F 1700.7 (8-69)

CAIT-UTC-NC60

Development and Validation of Methodologies for Rapid Inspection and Assessment of Fatigue Damage

FINAL REPORT

September 2020

Submitted by:

Sougata Roy, Ph.D.
Associate Research Professor
Department of Civil and Environmental Engineering

Center for Advanced Infrastructure and Transportation
Rutgers, the State University of New Jersey
100 Brett Road,
Piscataway, 08854

ABSTRACT

Causes of unusual fatigue cracking of a steel bridge owned by the New Jersey Turnpike Authority (NJTA) was investigated by Finite Element Analysis(FEA). The bridge is located on a strategic commerce route and is subjected to high Average Daily Truck Traffic (ADTT) consisting of significant fraction of overloaded trucks having Gross Vehicle Weight as high as twice the legal limit. The bridge originally built in 1950s and widened in 1971 is in service for more than 60 years. Fatigue cracking was observed in the top flange of the floor beams at deck expansion joints. The cracks developed at bearing stiffeners under the stringers and grew through the flange at some locations. Based on Weigh-in-Motion (WIM) studies performed at a nearby bridge, the bridge model was analyzed for 2.25 times the AASHTO fatigue design truck load plus 15% impact. The analysis showed that the maximum stress in the floor beam flange developed when the rear tandem axle of the truck loading crossed over to the deck on one side of the expansion joint. The maximum stress range occurred under the loaded bearing on the floor beam bracket, which was remnant from the original construction and was incorporated into the deck widening. The fatigue cracking in the flange adjacent to the bearing stiffeners was due to cyclic plastic straining. The local stresses at the holes for the bearing retaining bolts also exceed the yield limit of the material leading to fatigue cracks in the flange emanating from the holes. Due to significantly larger section modulus of the interior floor beam, the stresses in the flange was less than the AASHTO CAFT for Category A or base metal. No fatigue crack growth was observed nor was expected at this location. The analysis showed that the fatigue cracking was due to frequently occurring overloaded trucks in the truck traffic spectrum. The fatigue cracking was expected to be localized under the widened section of the bridge carrying the two exterior lanes mostly traversed by truck traffic, where the section modulus of the floor beam was significant less than that of the floor beams between the interior girders. Based on the findings, it is recommended that the exterior floor beam between the exterior and the first interior girder be strengthened to reduce the stresses in the flange below the CAFT of respective details.

ACKNOWLEDGEMENTS

The research presented in this report was sponsored by a grant received from the United States Department of Transportations, University Transportation Centers Program. The author gratefully acknowledges the support received for this study. The author is also grateful to Ms. Jean Laird and Mr. Bill Wilson of the New Jersey Turnpike Authority (NJTA) for providing access to all the information relevant to this study and for overall guidance and advice. Special thanks are also due to HNTB Corporation and GPI Inc. for help with providing necessary information and guidance for this study. Finally the author would like to thank Mr. Patrick Szary, and Ms. Marta Zurbriggen of the Center for Advanced Infrastructure and Transportation (CAIT) at Rutgers University for the administrative support.

LIST OF TABLES

LIST OF FIGURES

TABLE OF CONTENTS

1 INTRODUCTION

1.1 Background

The New Jersey Tunpike Authority (NJTA) owns several steel bridge superstructures that are in service for more than 60 years. Being on strategic commerce route, these bridges are subjected to large Average Daily Truck Traffic (ADTT), with potential for fatigue damage to the bridge superstructure. Recently unique fatigue cracking was discovered in one of the major bridges in the floor beams under the stringers at the deck expansion joints. The deck in this bridge is supported by four or six span continuous stringers resting on the floor beams. This fatigue cracking is unique in that the cracks developed in the floor beam top flange-to-floor beam web stiffener welds, either at the weld toes or from the weld root that eventually severed the stiffener-to-flange connection. Subsequently, fatigue cracking developed in the floor beam web gap at the stiffener due to unrestrained out-of-plane distortion of the floor beam web. This cracking was first discovered at the stringer locations under the left (or the slow) lanes, mostly traversed by truck traffic. Over the years, similar cracking developed at other stringer locations under the inner (fast) lanes.

Such pervasive fatigue cracking of stiffener-to-compression flange welds has not been reported in the literature. From the cracking mode it appears that the welds are subjected to a tensile stress that is prying open the connection. This would suggest a relative rotation of the floor beam flange (in the transverse direction of the floor beam) with respect to the stiffener. With the presence of back-to-back stiffeners welded to the flange under each stringer, however, such rotation does not appear to be possible. One possibility for this cracking is that the connections are experiencing unusual impact loading from the axle crossings at the deck joints. The impacts and subsequent vibrations with the passage of each vehicle, particularly heavy trucks, are perceptible.

Given a large number of these connections in the bridge and the unusual cracking mode, determining the root cause was necessary for an appropriate intervention plan and maintaining this structure on a regionally important corridor in a state of good repair. To this effect, a computational research was performed to determine the critical stresses at a typical connection detail in the bridge under simulated moving load. This study is presented in this report.

1.2 Research Objectives

The objectives of the study were:

(1) to investigate the root causes of the unusual fatigue cracking observed at the stiffener-to-flange welded connections in floor beams under stringers; and

(2) to decide an appropriate intervention plan for an unique but pervasive problem in an important bridge for maintaining in a state of good repair.

1.3 Research Approach

The causes of the unique fatigue cracking observed in the floorbeam-to-stiffener connections was evaluated by 3D Finite Element Analyses (FEA) of critical stresses under moving load. A part of the bridge was modeled and analyzed for site specific loading, simulating local response of the structure at the floorbeam-to-stiffener connections. The research objectives were accomplished by performing a series of sequential and interrelated tasks. The study was initiated by collecting and reviewing all relevant information related to the subject bridge including as-built drawings, inspection reports, crack locations and photographs. In addition, a NJTA commissioned detailed study related to fatigue investigation of another nearby bridge on the corridor was reviewed for site specific traffic spectrum and loading, and other pertinent field measurements. Based on review of available information, a strategic model of the bridge was developed consisting of half width of the bridge and a length extending over three floorbeams. The model was analyzed subject to site specific truck axle loading. The response of the bridge was assessed based on the analysis results and the causes of fatigue cracking was investigated. Based on the findings, an intervention strategy is proposed.

1.4 Report Organization

The report is divided into five sections. The current section or the first section discusses the background, describes the research objectives and approach and describes the organization of the report.

The second section reviews the available information including a description of the bridge, the details of cracking and a brief review of a relevant study of a nearby bridge.

The details of Finite Element Analysis (FEA) is presented in the third section.

The analysis results are discussed in the fourth section.

The conclusions, recommendations and future work are presented in the fifth and the final section.

2 REVIEW OF AVAILABLE INFORMATION

2.1 Description of the Bridge

The subject bridge is a multi-span steel girder-floor beam-stringer superstructure with concrete deck, with the stringers sitting on top of girder-floor beam framing and the concrete deck spanning between the stringers. The structure consists of a symmetric three span continuous (275-375-275 ft.) river crossing (with variable depth girders), and respectively 21 and 14 simply supported approach spans (with uniform depth girders) to the south and north of the river crossing. The approach spans ranged between 105 ft. to 170 ft. The bridge, built in 1951, was comprised of two girders spaced transversely at 56 ft. and varying overhangs, carrying two 36 ft. carriageways (one each) for bi-directional traffic. The steel superstructure was of riveted construction. In 1971, the bridge was widened using an additional welded weathering steel girder on each side of the bridge. The new girders were connected by new floor beams attached to the cantilever brackets of the original bridge. A typical cross section of the widened bridge is shown in Figure 2-1.

In 2011, the bridge deck was reconstructed. As part of this effort, the concrete bitumen filled deck joints were replaced by armored strip seal joints. In the river spans, the stringers were typically four span continuous over floor beams provided at 25 ft. centers, except over the interior pier where the stringers were six span continuous. The deck joints were provided at the discontinuous ends of the stringers. In the approach spans, the deck joints coincided with the simply supported girder ends over the piers. In addition to replacing deck joints, the stringers in the river span were replaced and were supported by steel reinforced elastomeric bearings on floor beams. These replacements were necessitated for addressing recurring failure of the stringer-to-floor beam connections in the river span and deteriorated stringer ends from leaky joints. In the original design, the stringers in the river span were $21WF62$ or $21WF73$ rolled sections having a depth of about 21 and $21.5\ in.$ respectively. The replaced stringers are $W18 \times 71$ rolled section having a depth of $18.5\ in.$ The reduced depth of the stringers was necessitated for accommodating reinforced elastomeric bearings including the sole and the base plates without elevating the roadway.

2.2 Details of Cracking

During the 2016 biennial inspection of the bridge, cracking in the floor beam stiffener-to-top flange welds and the adjacent floor beam web gap was discovered at stringers S2 and S3 (under the west 1971 widened section) and stringers S14 and S15 (under the east 1971 widened section) beneath all seven deck joints within the river spans. This cracking was not identified during the 2012 and 2014 biennial inspections. As evident from Figure 2-1, the subject stringers are located under the left most or the slow travel lane and the shoulder. Such cracking was not found at the outermost stringers S1 and S16 located under the parapet. The floor beam stiffeners in the widened part of the structure are $\frac{7}{16}\ in.$ plates welded to the top flange of the floor beam. In the original part of the structure the stiffeners are made of $5 \times 3\frac{1}{2}\ in.$ angles, with the longer leg protruding and milled to bear against the floor beam flanges, except for a few locations where the protruding leg of

the angles were welded to the top flange by repair plates (addressing corrosion damage). Cracking of the floor beam top flange at the stiffener connections in the original structure, both with milled to bear and welded details, was also observed under stringers S4 (west carriageway) and S13 (east carriageway). In addition, cracks were discovered in the flange initiating from the holes for the bearing retaining bolts. During subsequent inspections, crack growth was noted leading to severance of the floor beam stiffener-to-flange welds or fracture of the floor beam flange at many locations.

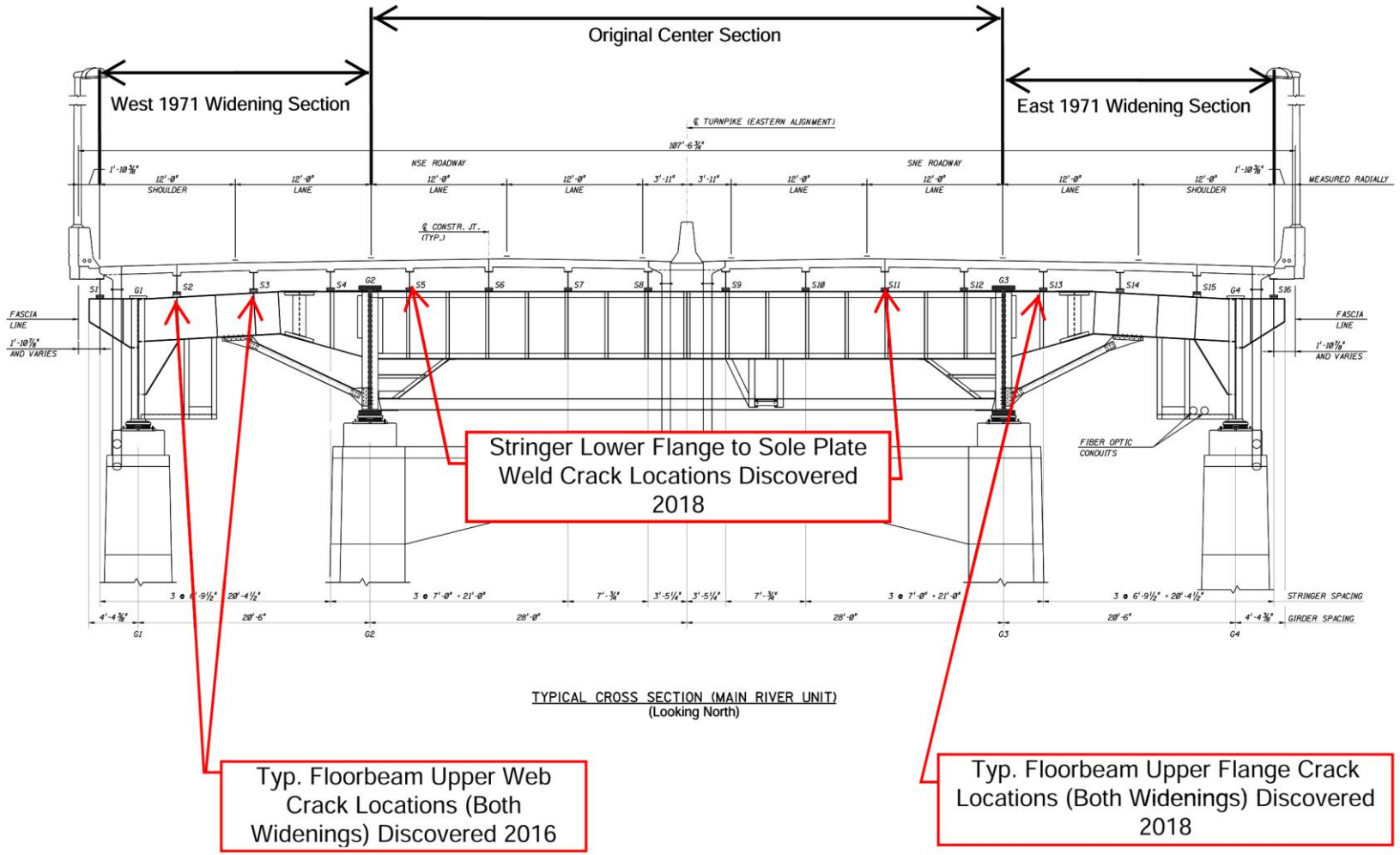

TYPICAL CROSS SECTION (MAIN RIVER UNIT)
(Looking North)

Figure 2-1 Cross section of bridge (taken from inspection report)

floor beam top flange-to-floor beam web stiffener welds, either at the weld toes or from the weld root that eventually severed the stiffener-to-flange connection.

2.3 Fatigue Study of a Nearby Bridge

A comprehensive study was undertaken by NJTA for a distressed nearby bridge that included a three pronged approach to better understand the response of the structure under vehicular traffic. This included a Weigh-in-Motion (WIM) study of data collected over 12 months, Structural Health Monitoring (SHM) of the bridge over discrete sections representing typical distressed structural details, and a detailed stress analysis of the bridge by finite element method. Although the cracking observed in the bridge for the current study is different than those observed in the nearby bridge, the study report was reviewed in detail particularly for the site-specific loading determined by the WIM studies. The relevant information are discussed further in Section 3.2.4.

3 DETAILS OF FINITE ELEMENT ANALYSIS

3.1 Modeling Approach

A part of the bridge was analyzed for determining by finite element method the critical stresses in the structure and the root cause of cracking.

Three dimensional simulation of the river spans for the entire bridge, consisting of three span continuous girders-floor beam-stringer system would be prohibitive. Although such a model seems exciting, the information provided would not be more valuable compared to that obtained from a part model of the structure, particularly with the prognosis that the local axle load effects are likely responsible for the observed fatigue cracking in the structure. Since the critical effect of axle loads on a floor beam occurs when the loads are within one stringer span on either side of the floor beam, a length of the bridge one and half stringer spans on either side of a floor beam under a typical deck joint (where the cracks in the floor beam were reported) was modeled. In the transverse direction, taking advantage of symmetry, the model included one carriageway width of the bridge extending from the exterior face of the outer barrier up to the middle of the interior barrier (or the middle of the floor beam between the two interior girders). The connections of interest were in the floor beam under the deck joint, and are thus sufficiently away from the model boundaries. Accordingly, the proposed model size was sufficient to minimize any boundary effects on the connections of interest.

The part of the structure modeled is identified in Figure 2-1 The west side of the bridge carrying the north bound carriageway was modeled. The model included girders G1 and G2, floor beams FB3, FB4 and FB5, and stringers S1to S8. The length of the model was 80 ft. and the width of the model was about 52 ft.

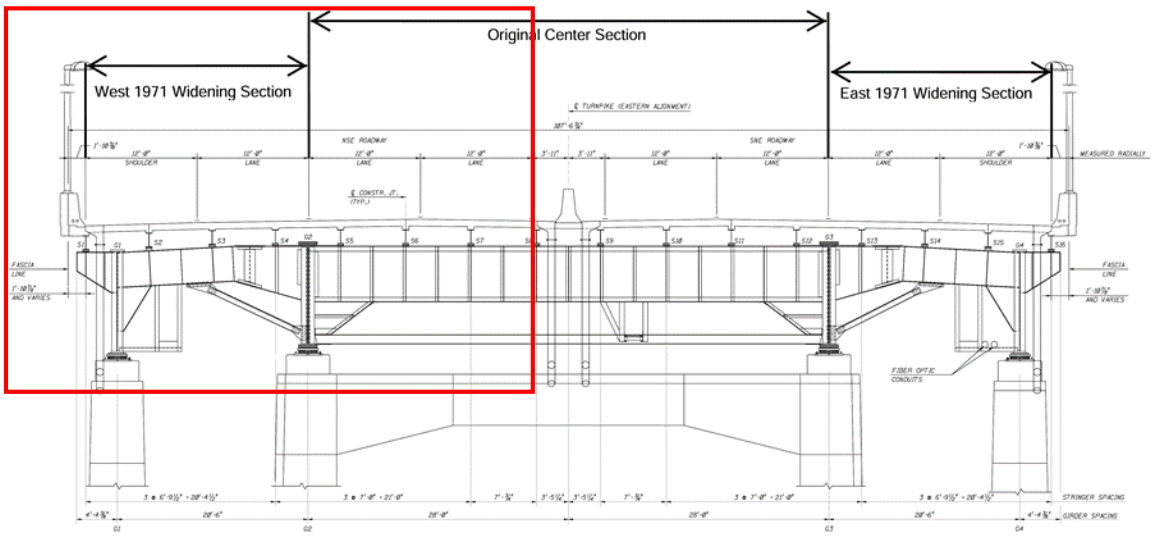

Figure 3-1 Cross section of bridge identifying the part modeled for FEA

3.2 Description of Model

3.2.1 Details of Bridge Model

A detailed 3D model was developed based on the design drawings of the bridge structure, including the changes due to the deck renovation undertaken in 2011. As described earlier, the girders are identical and of variable depth including both vertical camber on the top and draped profile on the bottom. The girder web depth over the modeled length, however, varied from $12\ ft\ 1\ in.$ at FB3, to $13\ ft. 2\frac{7}{8} in.$ at FB5, or, $1\ ft. 1\frac{7}{8}\ in.$ over 50 ft., resulting in a slope of about 1:43. This small variation was neglected and the girders were modeled for a uniform web depth of $12\ ft. 8\ in.$, the approximate web depth at FB4.

The north bound carriageway has cross slopes of 1.5% over the travel lanes and 3% over the shoulder. The composite reinforced concrete deck is uniform $8\frac{1}{2}\ in.$ thick. The cross slopes is achieved by sloping floor beams in the transverse direction and variable depth pedestals or bolsters under the stringers. In addition, the vertical profile and camber in the longitudinal direction is accommodated by variable haunch on top of the stringers. For the bridge model, the cross slope of the bridge in the transverse direction was neglected similar to the longitudinal direction. The floor beams were modeled horizontal. The top of all stringers was assumed to be at the same level. A uniform square haunch of $1\frac{1}{2}\ in.$ depth was modeled on top of the stringers. A uniform concrete deck of $8\frac{1}{2}\ in.$ was modeled on top of the haunch. Although for the physical structure the haunch depth varied from $0\ to\ 8\ in.$, the $1\frac{1}{2}\ in.$ haunch depth was selected as the most common haunch depth in the structure, creating a total 10 in. depth from the top of the stringer to the top of the concrete deck. The concrete parapet on the fascia side (west) was modeled, however, the concrete barrier on the median was not included.

The stringers are supported on reinforced elastomeric bearings and steel bolters on top of the floor beams. The bearings were modeled separately, and the sole and base plates were modeled integral with the bolsters. Any variation due to stringer depth and bearing height was accommodated by varying the height of bolsters.

A realistic model was developed based on the design drawings of the original superstructure from 1951, subsequent deck widening of 1971, and the redecking of 2011. All features of the structure were modeled. The knee braces to the floor beams and the bottom lateral bracings were included. In addition, the floor beam strengthening strut, connecting G2 and the floor beam between G1 and G2 at FB3, was included. The transverse stiffeners, connection angles, fill and shim plates, tie plates, gusset plates, splice plates and other attachments were considered as integral with the primary members. The riveted, bolted or welded connections were not modeled. The bolted connections at the bearings were also not modeled. All connections between different members were simulated as tie constraints.

Views of the bridge model are presented in Figure 3-11.

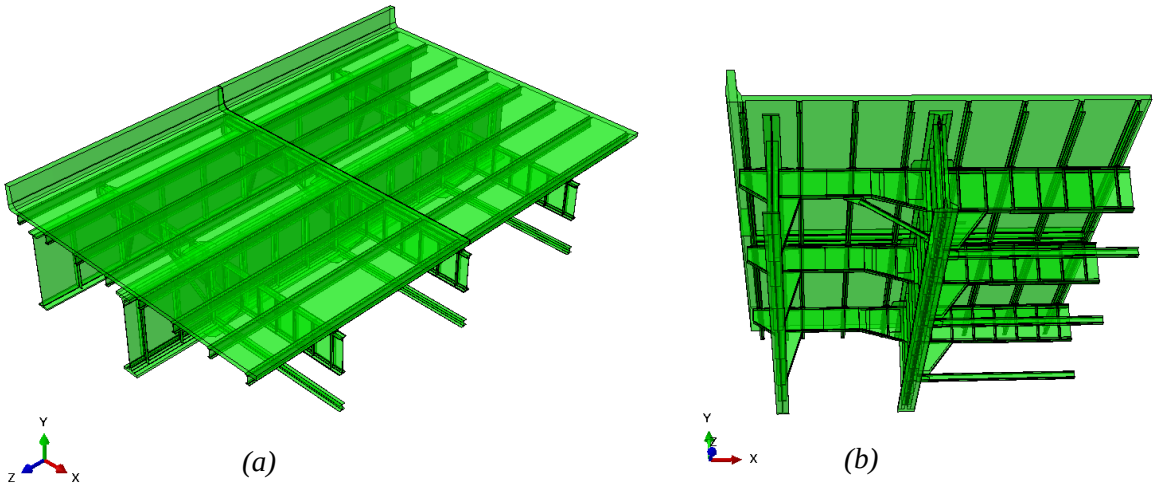

Figure 3-2 3D views of the bridge model: (a) isometric; (b) underside

3.2.2 Material Properties

Widely accepted linear elastic material properties of steel and concrete were used for analysis. The modulus of elasticity and Poisson's ratio of steel were assumed respectively as 29000 ksi and 0.3. These parameters for the deck concrete were considered as 2900 ksi and 0.15, respectively. The elastomeric bearings were modeled as hyperelastic material with near incompressible behavior. A composite shear modulus of 1.8 ksi, including the elastomer and the reinforcements, was assumed for the bearings. The Poisson's ratio was taken as 0.45.

3.2.3 Boundary Conditions

The model was analyzed for a fixed continuity boundary condition, where the displacements at the cut (or continuity) ends of the bridge were assumed to be zero. While the physical structure is expected to have non-zero displacements due to continuity at the cut boundaries, these global displacements were of little consequence on the local deformation under the wheel loads, which were of interest for this study.

3.2.4 Loading

The model was analyzed to simulated the effect of a site-specific truck load crossing the bridge. Based on Weigh-in-Motion (WIM) studies performed at a nearby bridge on the same corridor, the most frequent truck in the vehicle spectrum was of FHWA vehicle Class 9 (single trailer 5 axle truck of 3S2 configuration), constituting about 45% of the total truck traffic. This class of trucks also exceeded the Gross Vehicle Weight (GVW) the most, about 42% of the overall overweight truck traffic. Trucks of FHWA vehicle classes 6, 7 and 9 constituted the majority of the trucks on the bridge, for which GVW as high as 160 kip was recorded during the WIM study.

The root mean cube effective GVW for the north and the south bound truck spectrum was respectively 52 and 60 kips or, 0.72 and 0.83 of the GVW of a HL-93 design truck of the AASHTO LRFD Bridge Design Specifications (BDS) i.e., 72 kips. It may be

noted that in the current specifications this ratio is implicitly assumed to be 0.8 for the AASHTO fatigue truck. Thus, it may be concluded that the site specific loading on the subject bridge created similar effective stress range as the AASHTO fatigue design truck. The maximum measured GVW, however, was greater than three times the AASHTO fatigue design truck. The maximum GVW for the fatigue truck is implicitly considered as 1.75 times the AASHTO fatigue design truck in the current AASHTO BDS. In the previous editions of the specifications the maximum GVW was assumed to be 1.5 times the AASHTO fatigue design truck. Thus, it is evident that the bridge is traversed by trucks much heavier the design truck.

Since the local response of the structure under axle loads are of interest for the current study, the site specific axle loads were examined further. The distribution of

Table 3-1 Truck Axle Weight Distribution from WIM – North Bound

Axle Load Bin	Mean Axle Load/Bin P_i (lb)	Axle Load Count n_i	Frequency $f_i = \frac{n_i}{\sum_i n_i}$	$\sum_i f_i P_i^3$	Exceedance $\sum_i n_i(P_i > P_{Li})$	Exceedance (%)
0-5	2.5	830421	6.804E-02	1.06	12205027	100.000
5-10	7.5	4597997	3.767E-01	158.93	11374606	93.196
10-15	12.5	4497277	3.685E-01	719.68	6776609	55.523
15-20	17.5	2068216	1.695E-01	908.18	2279332	18.675
20-25	22.5	180281	1.477E-02	168.25	211116	1.730
25-30	27.5	26971	2.210E-03	45.96	30835	0.253
30-35	32.5	3120	2.556E-04	8.78	3864	0.032
35-40	37.5	497	4.072E-05	2.15	744	0.006
40-45	42.5	139	1.139E-05	0.87	247	0.002
45-50	47.5	108	8.849E-06	0.95	108	0.001
	$\sum$	12205027		2014.81		

P_{eff}=12.6 kip

Table 3-2 Truck Axle Weight Distribution from WIM – South Bound

Axle Load Bin	Mean Axle Load/Bin P_i (lb)	Axle Load Count n_i	Frequency $f_i = \frac{n_i}{\sum_i n_i}$	$\sum_i f_i P_i^3$	Exceedance $\sum_i n_i(P_i > P_{Li})$	Exceedance (%)
0-5	2.5	1779157	1.324E-01	2.07	13434368	100.000
5-10	7.5	6257162	4.658E-01	196.49	11655211	86.757
10-15	12.5	3647020	2.715E-01	530.21	5398049	40.181
15-20	17.5	1447469	1.077E-01	577.44	1751029	13.034
20-25	22.5	231768	1.725E-02	196.51	303560	2.260
25-30	27.5	63248	4.708E-03	97.91	71792	0.534
30-35	32.5	7947	5.915E-04	20.31	8544	0.064
35-40	37.5	463	3.446E-05	1.82	597	0.004
40-45	42.5	79	5.880E-06	0.45	134	0.001
45-50	47.5	55	4.094E-06	0.44	55	0.000
	$\sum$	13434368		1623.65		

P_{eff}=11.8 kip

measured axle weights for the north and the south bound trucks are shown respectively in Table 3-2 and Table 3-1. Axle weight as high as 50 kip was measured. The HL-93 notional truck consists of three axles, one 8 kip axle followed by two 32 kip axles that for fatigue design are spaced 30.0 ft. apart. As noted earlier, the GVW of a fatigue truck is implicitly assumed to be 57.6 kip i.e., each rear axle weighing 25.6 kip. With tandem configuration the weight of each axle in the rear axle group is 12.8 kip. Thus, the maximum measured axle load is about four times that of a AASHTO fatigue truck. For the north and south bound trucks, estimated root mean cube (RMC) effective (measured) axle load, as

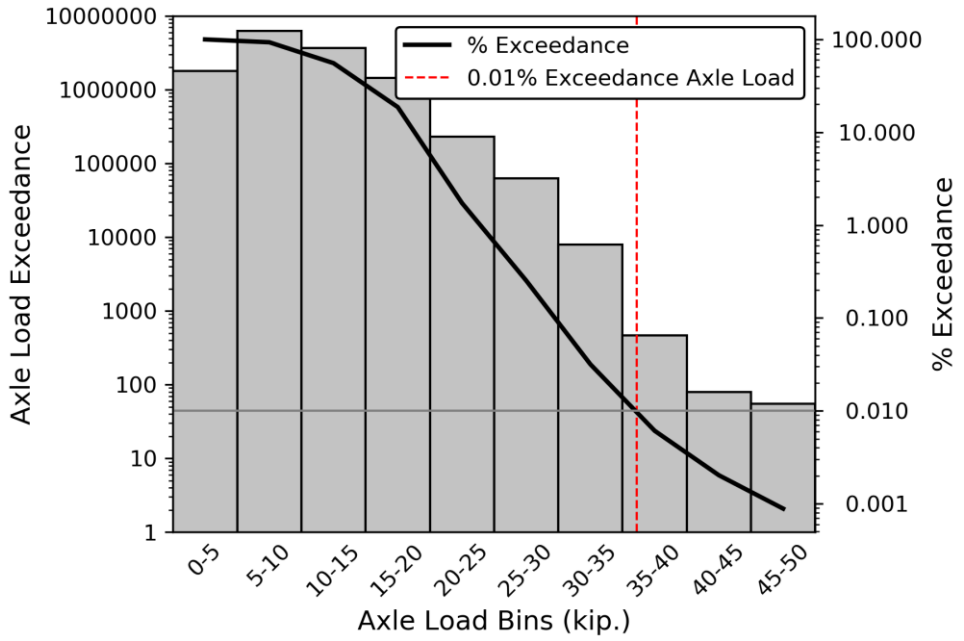

Figure 3-3 Exceedance histogram for north bound truck axles

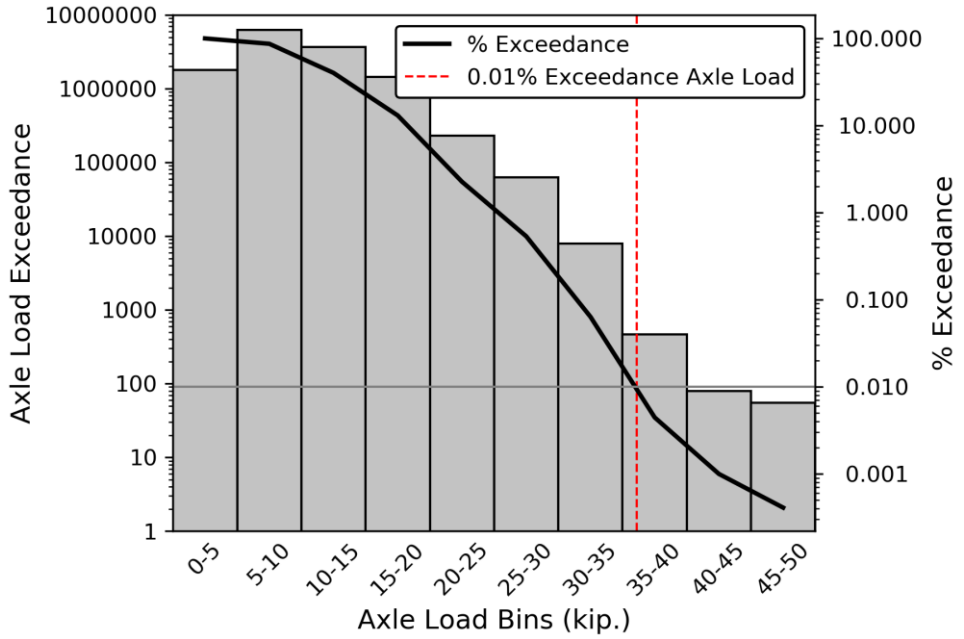

Figure 3-4 Exceedance histogram for south bound truck axles

presented in the tables, are respectively 12.6 and 11.8 kip. Assuming a linear relationship between the load and the resulting stress, and a linear accumulation of fatigue damage as proposed by Miner [1], this RMC effective axle weight can be considered as a representative of the measured variable axle weight spectrum. Also shown in the tables are the exceedances of each axle weight bin. The exceedance histograms for the north and south bound truck axle loads are presented respectively in Figure 3-3 and Figure 3-4. The percentage exceedance of the axle load bins is overlaid on the axle load exceedance histograms. For both direction truck traffic, the axle weight corresponding to 1 in 10,000 or 0.01% exceedance was about 36 kips. Research [2] has shown that stress range exceeding the constant amplitude fatigue threshold (CAFT) of a detail at a frequency greater than 1 in 10,000 contribute to fatigue damage at the detail. Assuming the stress produced is proportional to the load for linear elastic response, it can be reasoned that the load corresponding to the 1 in 10,000 or 0.01% exceedance is the limiting load, which if exceeded at a greater frequency will result in fatigue damage. In other words, the live load stress produced by this axle load should not exceed the CAFT of a detail for infinite fatigue life. From the analysis it is evident that this site specific limiting axle load is about three times the rear axle load of an AASHTO fatigue truck with tandem configuration.

To investigate the site-specific load effects, the bridge model was analyzed for the simulated passage of the rear axle of a HL-93 fatigue design truck of the AASHTO LRFD BDS. Since the trucks belonging to FHWA Vehicle Class 9 were the most demanding (in volume and weight), consideration of the HL-93 truck with a 30.0 ft. rear axle spacing, which is the notional representation of a tractor semi-trailer of 3S2 configuration (total 5 axles) within FHWA Vehicle Class 9, for analysis was appropriate. It is well known from field measurements, laboratory studies and other research that the response of a floor beam is primarily influenced by the axles that exist within the tributary area of the floor beam. For typical floor beam spacing of 25 ft., each floor beam would be influenced by one axle of the HL93 truck at a time. For more realistic representation, however, the rear axle of the HL-93 truck was split into a tandem configuration, as is recommended by the AASHTO LRFD BDS for analysis of steel orthotropic bridge decks. Accordingly, each tandem axle consisted of four tire contact areas, 4 and 6 ft. apart respectively in the longitudinal and transverse directions. As recommended by the AASHTO LRFD BDS, each tire contact area was considered as 10 in.×20 in., with the 10 in. dimension parallel to the traffic direction. Consistent with the site specific axle loads, as presented in the previous paragraph, the analysis was performed for 3×HL-93 loading for determining the most critical effects. A dynamic amplification or impact of 15% was also considered as specified by the AASHTO BDS for fatigue loading. This resulted in a pressure of 103.5 psi on the tire contact area.

The passage of the tandem axle across the bridge was discretized by four longitudinal and three transverse positions The four longitudinal positions were as follows:

1) Longitudinal position L1: The tandem axle was positioned symmetric about the deck expansion joint at FB4 in the longitudinal direction, i.e., each axle of the tandem was at 2 ft. from the center line of FB4.

2) Longitudinal position L2: The tandem axle was positioned such that the tire contact of the trailing axle abutted the expansion joint, but remained on the

deck to the north of the expansion joint, i.e., the axle was at 5 in. from the center line of FB4.

3) Longitudinal position L3: The tandem axle was positioned such that the trailing axle crossed over on to the deck to the south of the expansion joint, and the tire contact of the trailing axle abutted the expansion joint i.e., the axle was at 5 in. from the center line of FB4.

4) Longitudinal position L4: The trailing axle of the tandem was at 2 ft. from the center line of FB4.

The three transverse positions were as follows:

1) Transverse position T1: The tandem axles were positioned such that the east side wheels were centered on girder G2, and the west side wheels were at 6 ft. towards girder G1.

2) Transverse position T2: The tandem axles were positioned symmetrically about girder G2 in the transverse direction, i.e., the east and west wheels were at 3 ft. from the girder centerline.

3) Transverse position T3: The tandem axles were positioned such that the west side wheels were centered on girder G2, and the east side wheels were at 6 ft. towards girder G3.

Combining the four longitudinal and three transverse positions, the model was analyzed for 12 load cases. As is evident from Figure 2-1, the physical lane marking on the bridge between the left most lane or the slow lane and the adjacent interior lane matched with the centerline of G2. It was anticipated that the most critical loading on the bridge occurred due to truck traffic primarily on these two lanes. Accordingly, the load positions were chosen to identify the critical stresses developed locally in FB4 under stringers S4

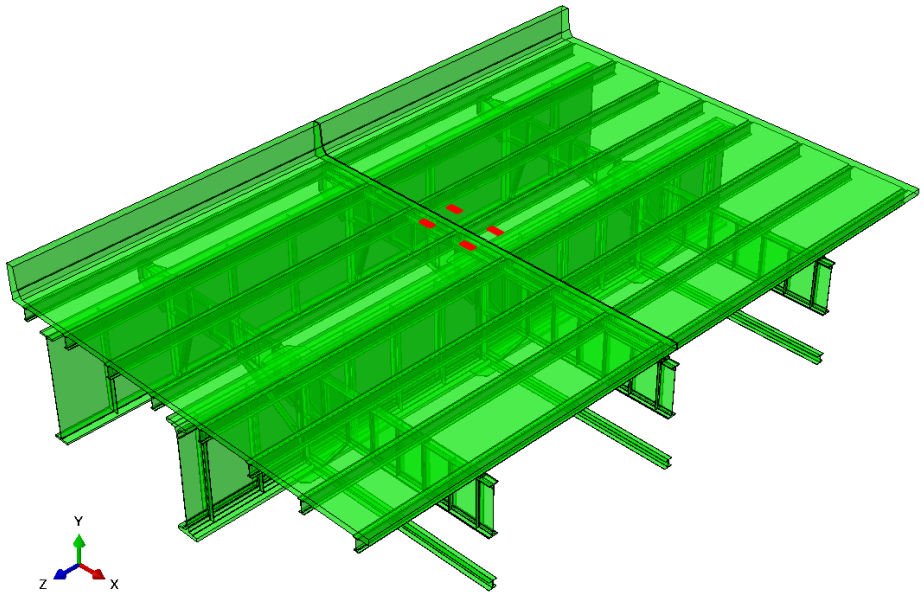

Figure 3-5 Load position L1T1

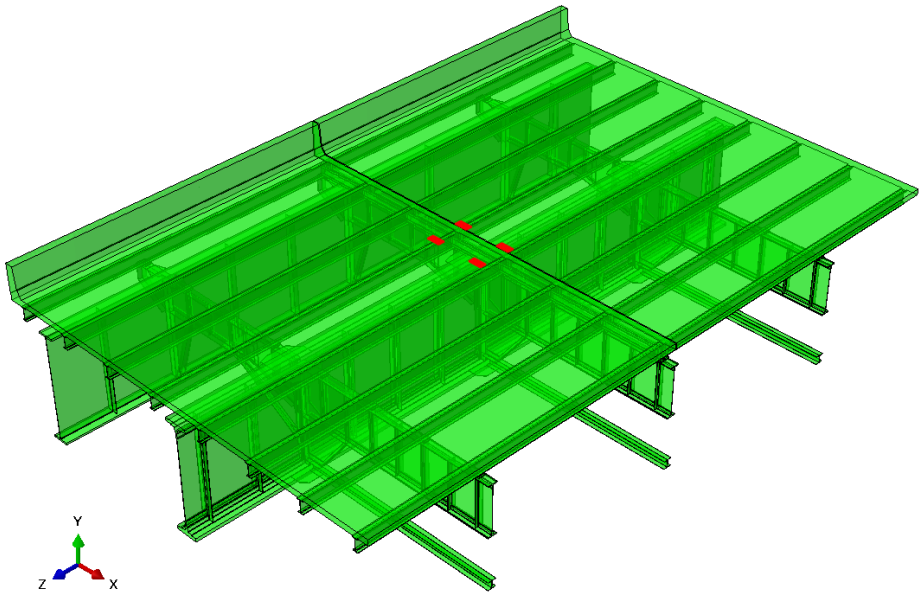

Figure 3-6 Load position L2T2

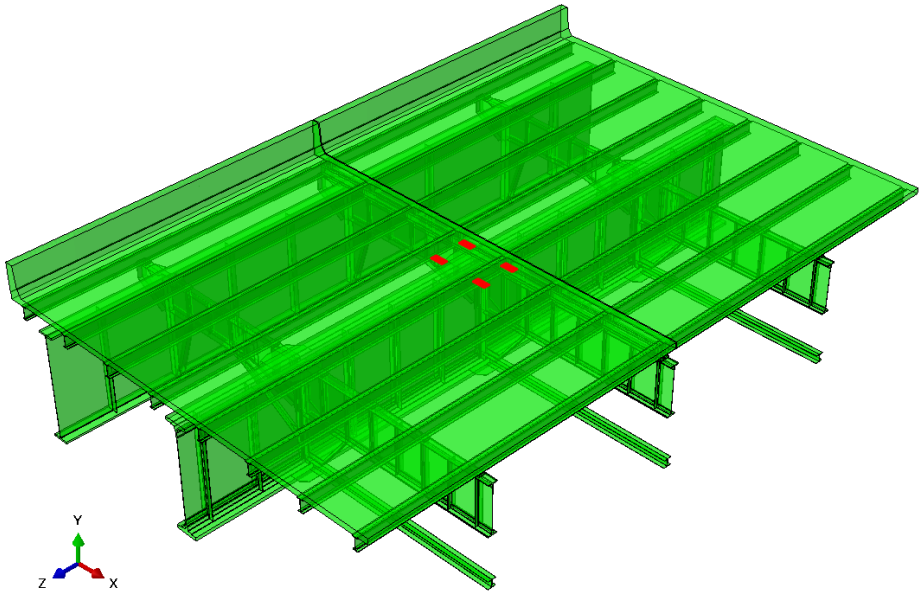

Figure 3-7 Load position L4T3

and S5 when the truck traffic traversed along and straddled across these two lanes. The load cases were identified by combining the corresponding longitudinal and transverse positions. For example, load case L2T3 corresponded to longitudinal position L2 and transverse position T3. A few load positions are shown in Figures 3-3, 3-4, 3-5 and 3-6.

3.2.5 Elements

The bridge model was discretized (meshed) with 3D hexahedral elements, incorporating twenty node, quadratic, reduced integration, isoparametric formulation. The

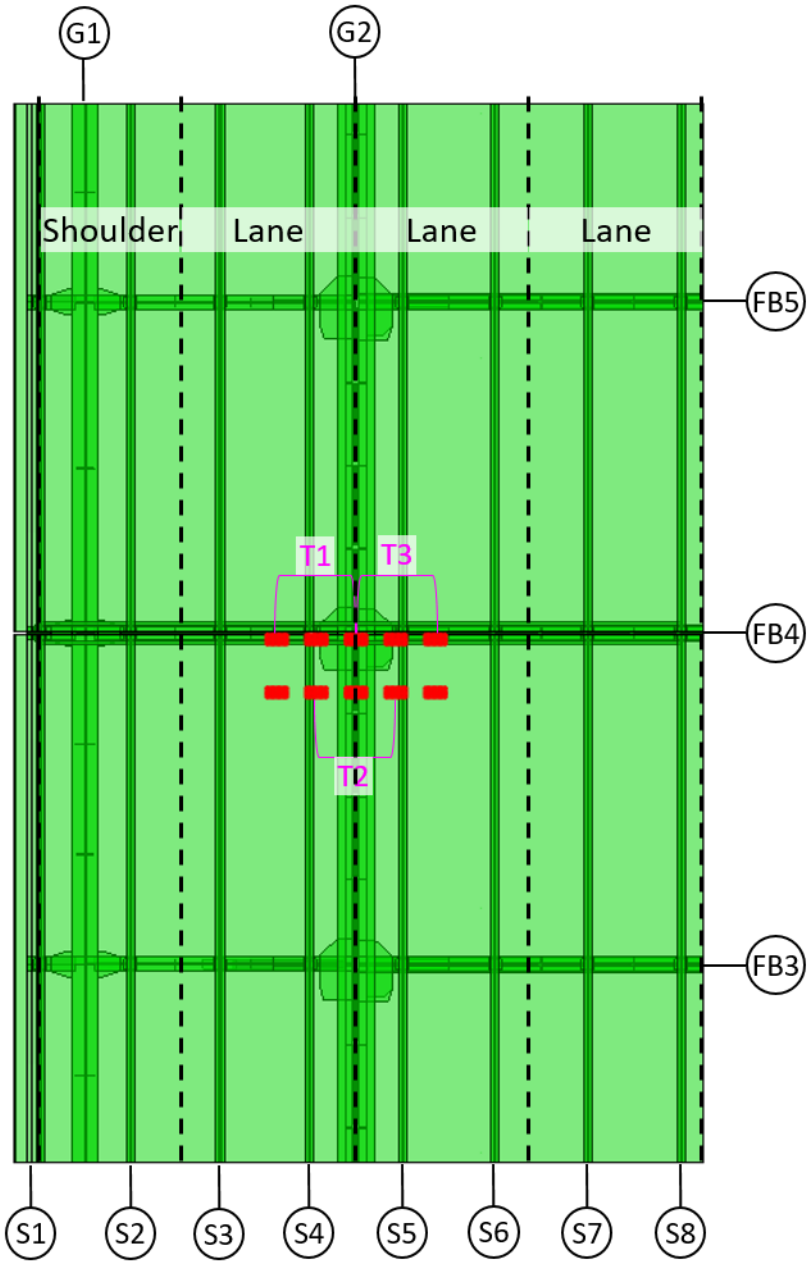

Figure 3-8 L3 load positions

model contained 4,925,058 nodes and 917,109 elements, generating 14,803,104 solution variables.

3.2.6 Analyses

The analyses were executed parallel on a distributed memory computer cluster of up to two nodes, each having 8 central processing units (CPU) and employing direct solver algorithm. All analyses were linear elastic.

3.3 Analysis Results

Presentation of the analysis results are focused mostly on the stresses in the floor beam flange adjacent to the stringer bearings, where cracking is observed in the field. The analysis showed that for all load cases the tandem axles produced critical stresses in the top flange of FB4 under the bearings for stringer S4. High localized stresses were also observed in the top flange of FB4 under S5, however, these stresses were significantly less. The maximum stresses in FB4 flange occurred under longitudinal load position L3, when the trailing axle of the tandem crossed over the expansion joint. In this case, the floor beam was loaded only by the south side bearings. Although stringers S4 and S5 were directly under the wheel path in load position L3T2 (see Figure 3-8), the maximum stress under S4 occurred in load case L3T1 and the maximum stress under S5 occurred in load case L3T3.

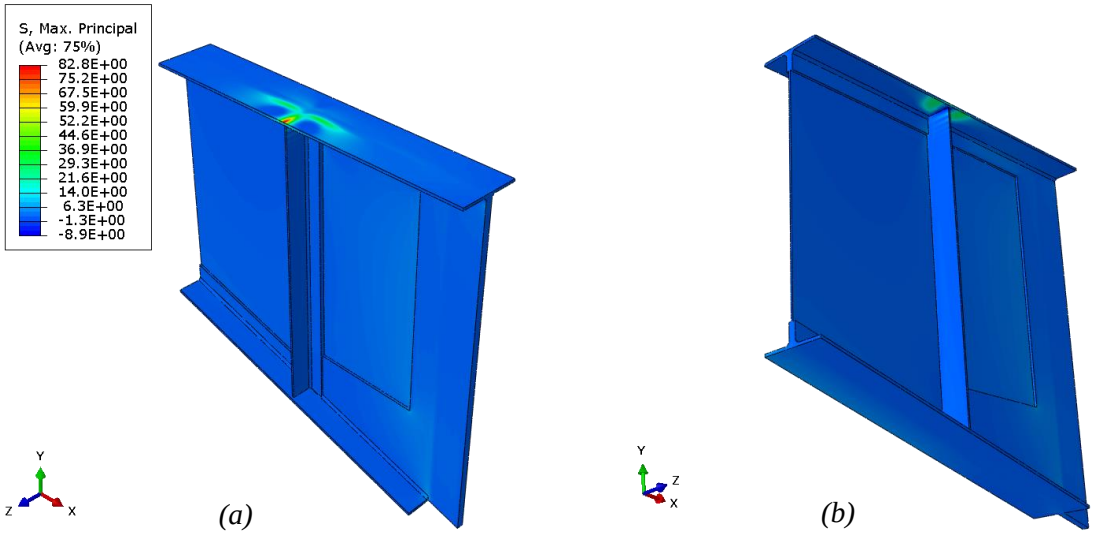

Figure 3-9 Contour of maximum principal stress in FB4 bracket for load case L3T1: (a) view from top; (b) view from bottom

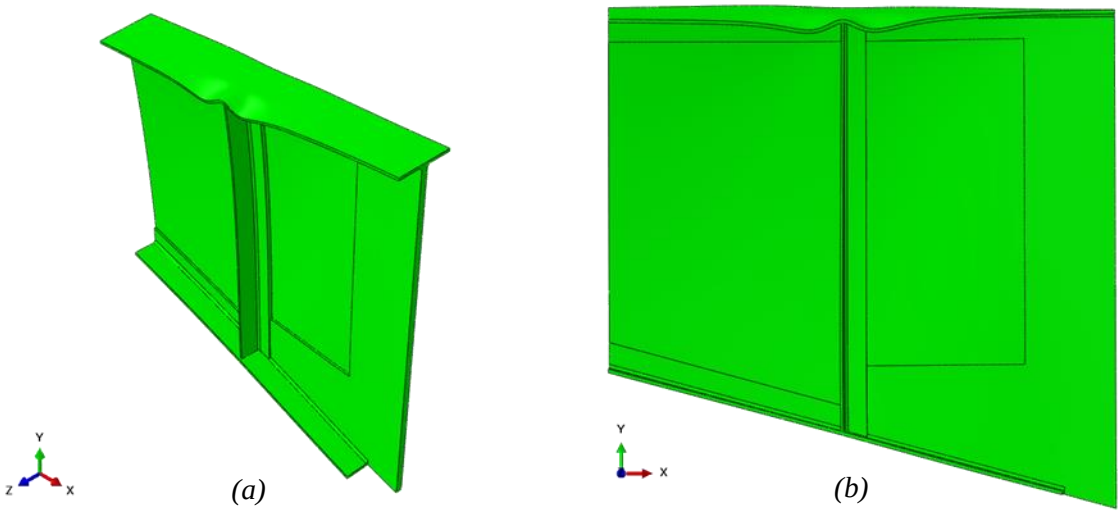

Figure 3-10 Deformation of FB4 bracket for load case L3T1 (50×): (a) isometric view; (b) south elevation

It is likely that the stringers S4 and S5 were influenced by the both side wheels, respectively for transverse load positions T1 and T3. In other words, both side wheels were within the tributary areas of the S4 and S5 for transverse load positions T1 and T3 respectively. Whereas, for transverse position T2, only one side wheels were within the influence region of the stringers. Indeed, the loads from the bearings onto the flange, as obtained from the analysis results for the three transvers positions for longitudinal position L3, confirm this assessment (see Table 3-3)

Table 3-3 Load from South Bearing onto FB4 Flange

Bearing Under	Bearing Loads for Load Positions (kip)		
	L3T1	L3T2	L3T3
S4	37.8	31.8	20.1
S5	22.0	34.5	40.6

Contour plots of the maximum principal stress in the top flange of FB4 bracket under S4 are shown in Figure 3-9 for the load case L3T1. Only the FB4 bracket (retained from the original construction) is shown for clarity. The high local stresses occurred due to bending of the top flange under S4 south bearing, as shown in Figure 3-10. The flange of the built-up FB4 bracket is made of two back-to-back $6 \times 4 \times \frac{1}{2}$ angles, with the 6 in. leg forming the flange. The flange angle leg is subjected to negative moment at the bearing stiffener ($5 \times 3\frac{1}{2} \times \frac{3}{8}$ angles with the 5 in. leg protruding), and positive moment away from it. As can be seen, due to the eccentric loading on the south bearing of S4 (since the tandem axle is entirely on the deck south of the expansion joint in load case L3T1), the FB4 is experiencing some twisting deformation. Note that the deformation is shown in Figure 3-10 at 50× magnification.

The maximum principal stress field in the top flange of FB4 bracket is further presented in Figure 3-11 to demonstrate the magnitude and direction. As is evident, the

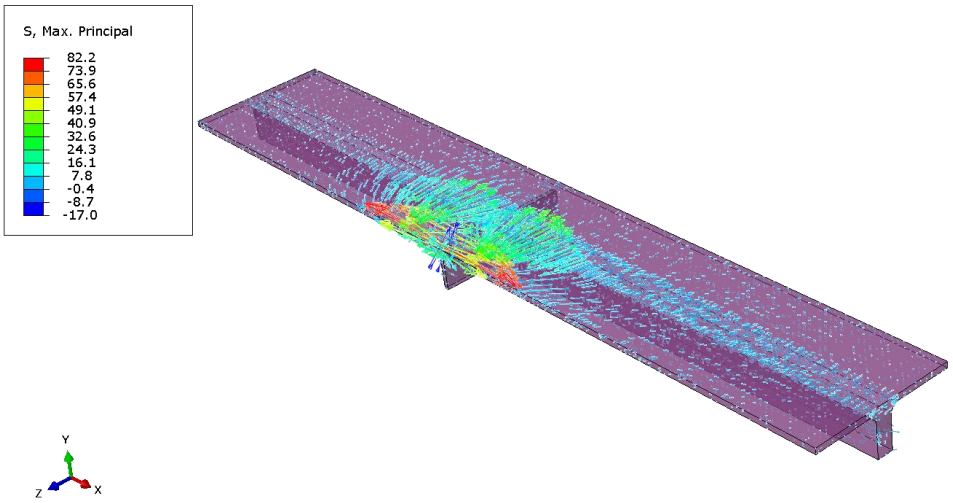

Figure 3-11 Maximum principal stress field in the top flange of FB4 bracket for load case L3T1

maxima of principal stress, occurring over the bearing stiffener near the free edge of the flange was primarily along the flange or in the x-direction. Inside the flange, maximum principal stress of smaller magnitude occurred in the transverse direction of FB4, consistent with the bending of the flange like a cantilever supported on the web.

The plot of longitudinal stress S_{11}, along longitudinal paths on the top and the bottom of the flange (on the same vertical plane, adjacent to the free edge) towards the south side or the loaded span are shown in Figure 3-12. The plot is prepared with the centerline of the bearing stiffener protruding leg (considered as the centerline of the bearing stiffener) as origin, which also coincided with the centerline of S4. The distances are considered positive and negative respectively towards G2 and G1. The stresses were consistent with the bending behavior presented earlier. Stresses of almost equal magnitude and opposite signs were noted on the top and the bottom path, suggesting predominantly flexural deformation of the floor beam flange under the S4 bearing. The floor beam flange (protruding leg of the angle) experienced reverse flexure, with concave deformation over the bearing stiffener angle, rapidly changing to convex deformation under the bearing

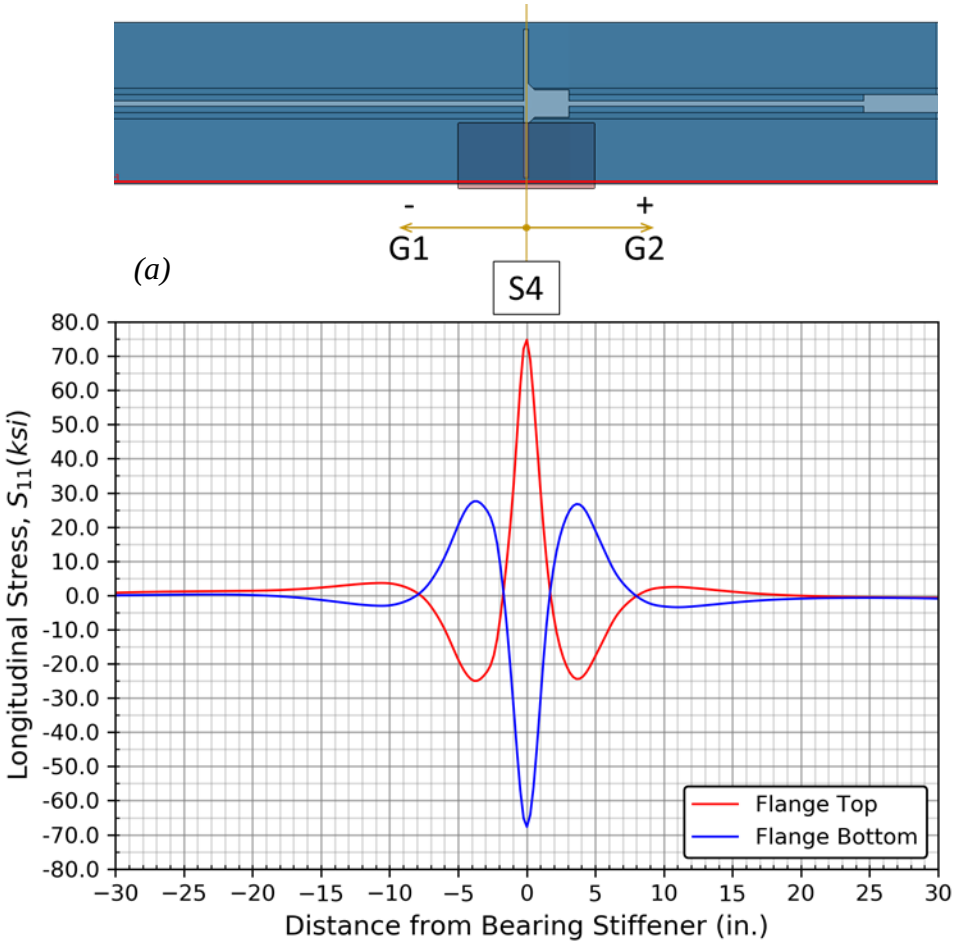

Figure 3-12 Longitudinal stress in the top flange of FB4 bracket for load case L3T1: (a) plan view of top flange showing path and origin; (b) plot of longitudianl stress along path

footprint. The maximum tensile stress on top of the flange, occurring at the centerline of the bearing stiffener, is about 75 ksi (assuming elastic behavior), which significantly exceeded the yield strength of the material, assumed 36 ksi for the carbon steel that is specified in the original bridge plans. The maximum tensile stress at the bottom of the flange is about 25 ksi, which occurred at about 4 in. from the stiffener centerline. Note that the bearing is $10\frac{1}{2}\ in.$ wide and the bearing retaining bolts are located $2\frac{1}{2} in.$ from the centerline of the bearing stiffener. The tensile stress in the flange at the bolt holes is about 20 ksi. Considering stress concentration, the local stress at the edge of the hole likely exceeded the yield stress of the material (assumed 36 ksi).

The variation of vertical stress (stress in the Y or 2-2 direction), S_{22} at the bearing stiffener-to-flange interface is presented in Figure 3-13. The stresses are determined on a path along the centerline of the protruding leg of the bearing stiffener angle. The plot is prepared with respect to the centerline of FB4 as origin. The distances are considered positive and negative respectively towards south and north, i.e., towards FB3 and FB5. The south bearing stiffener under the loaded S4 bearing experienced bilinear compressive stress distribution that increased at a flatter rate up to about $4\frac{1}{2}\ in$ from the centerline of the floor beam web and then at a much rapid rate. The maximum compressive stress occurring at the edge of the bearing stiffener was about 22 ksi. The stress at the north bearing stiffener-to-top flange interface under the unloaded S4 bearing was insignificant. The north bearing stiffener, however, experienced tensile stresses as the floor beam twisted due to the eccentric loading.

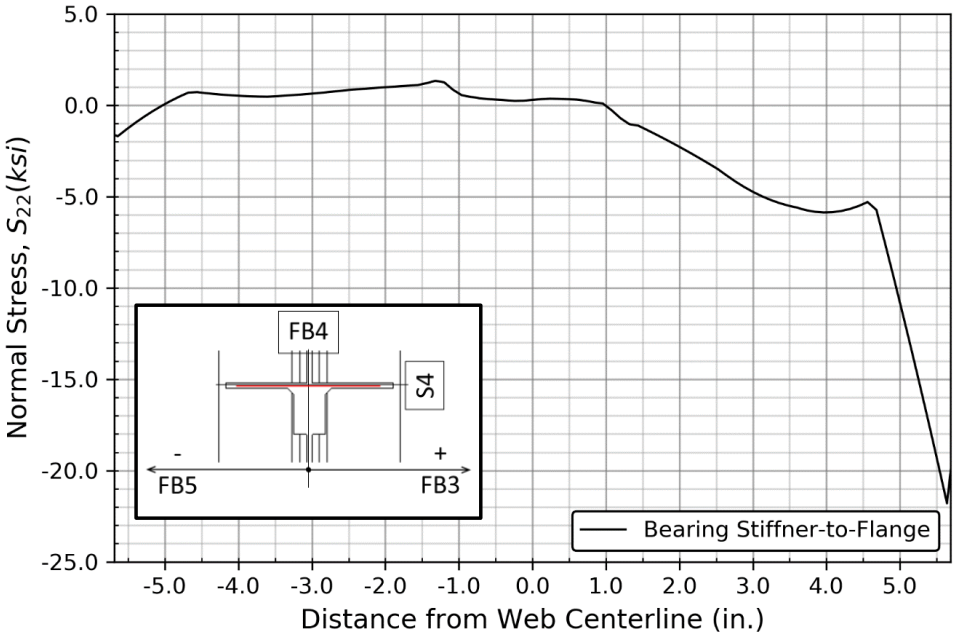

Figure 3-13 Vertical stress along path at soffit of FB4 top flange and the centerline of bearing stiffener under S4 for load case L3T1

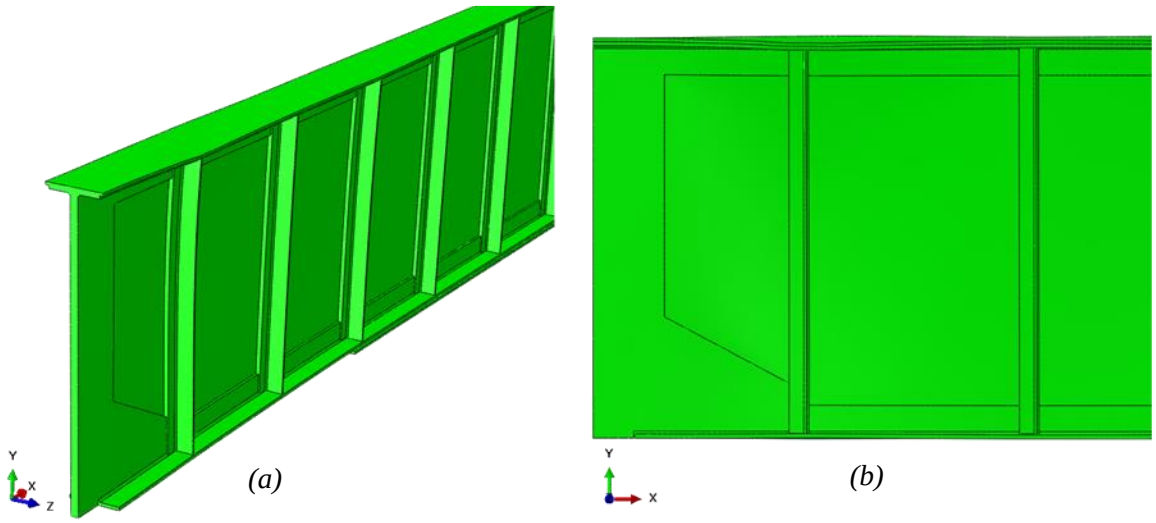

Figure 3-14 Deformation of FB4 interior for load case L3T3 (50×): (a) isometric view; (b) south elevation

The maximum stress in FB4 flange under S5 occurred in load case L3T3. Contour plots of the maximum principal stress in FB4 for this load case are shown in **Error! Reference source not found.**. Only the part of the floor beam between G2 and G3 is shown for clarity. The deformation of the floor beam at 50× magnification is shown in Figure 3-14. Local bending of the flange under the bearing for S5 was noted that resulted in the maximum flange stresses. The response of the floor beam flange was similar to that under S4. The deformation was localized only under the south bearing, since the entire tandem was on the south side of the expansion joint (see Figure 3-8) and some twisting of the floor beam was noted due to this eccentric loading. The flange of the floor beam between G2 and G3 was built up of two back-to-back $6 \times 6 \times \frac{3}{4}$ inch angles and a $14 \times \frac{5}{8}$ in. cover plate.

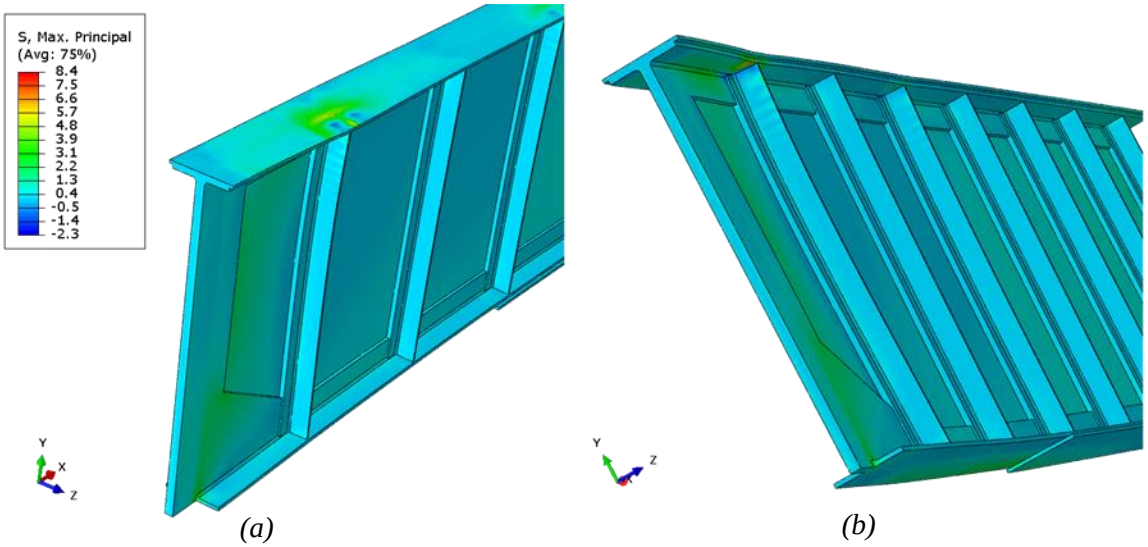

Figure 3-15 Contour of maximum principal stress in FB4 interior for load case L3T3: (a) view from top; (b) view from bottom

The flange was subjected to deformation concave down at the bearing stiffener ($5 \times 3\frac{1}{2} \times \frac{3}{8}$ in. angles with the 5 in. leg protruding), and convex up away from it.

The direction and magnitude of maximum principal stress in the top flange of FB4 between G2 and G3 is presented in Figure 3-16. Compared the distribution of principal stress under S4 as presented earlier, the stresses under S5 are more complex. Looking at the distribution of principal stresses in three orthogonal views (in X, Y, and Z –directions), it is evident that the maxima of principal stress is not oriented along the flange, but in the transverse direction at an angle. Maximum principal stress of comparable magnitude was also observed in the longitudinal direction (X or 1 direction), but at an angle with the flange plane. This complex distribution of maximum principal stresses under the S5 bearing

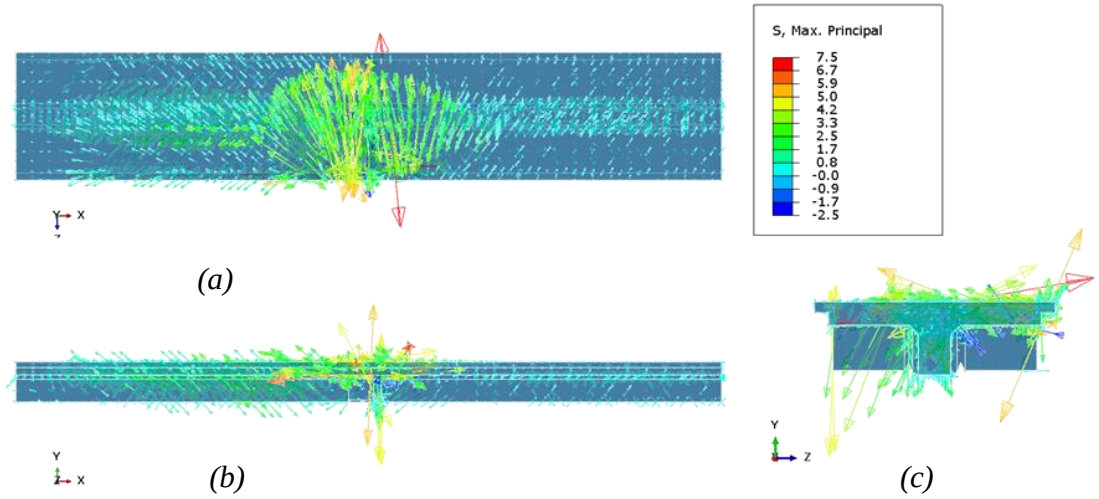

Figure 3-16 Maximum principal stress field in top flange of FB4 interior for load case L3T3: (a) plan view; (b) elevation view; (c) section view

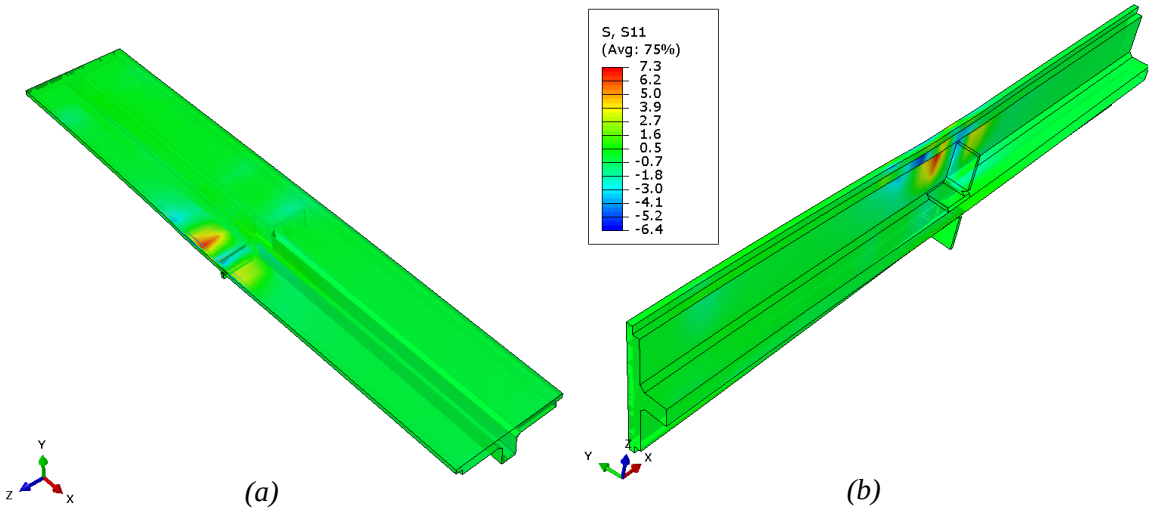

Figure 3-17 Contour of longitudinal stress in the top flange of FB4 interior for load case L3T3: (a) view from top; (b) view from bottom

suggests existence of high shear stresses between the bearing stiffener and the flange, and the local flange bending was predominantly in the transverse direction. High maximum principal stress was also observed in the vertical direction (Y or 2 direction) at the bearing stiffeners under the S5 bearings.

The contour plot of longitudinal stress S_{11} in the floor beam flange adjacent to S5 bearing is presented in Figure 3-17. Variation of longitudinal stress along longitudinal paths on the top of the flange plate and the bottom of the connection angle (on the same vertical plane, adjacent to the protruding leg of the bearing stiffener angle) towards the south side or the loaded span is shown in Figure 3-18. The plot is prepared with the centerline of the bearing stiffener protruding leg (considered as the centerline of the bearing stiffener) as origin, which also coincided with the centerline of S5. The distances are considered positive and negative respectively towards G3 and G2. The variation of longitudinal stresses were consistent with the bending behavior presented earlier. Stresses of almost equal magnitude and opposite signs were noted on the top and the bottom path,

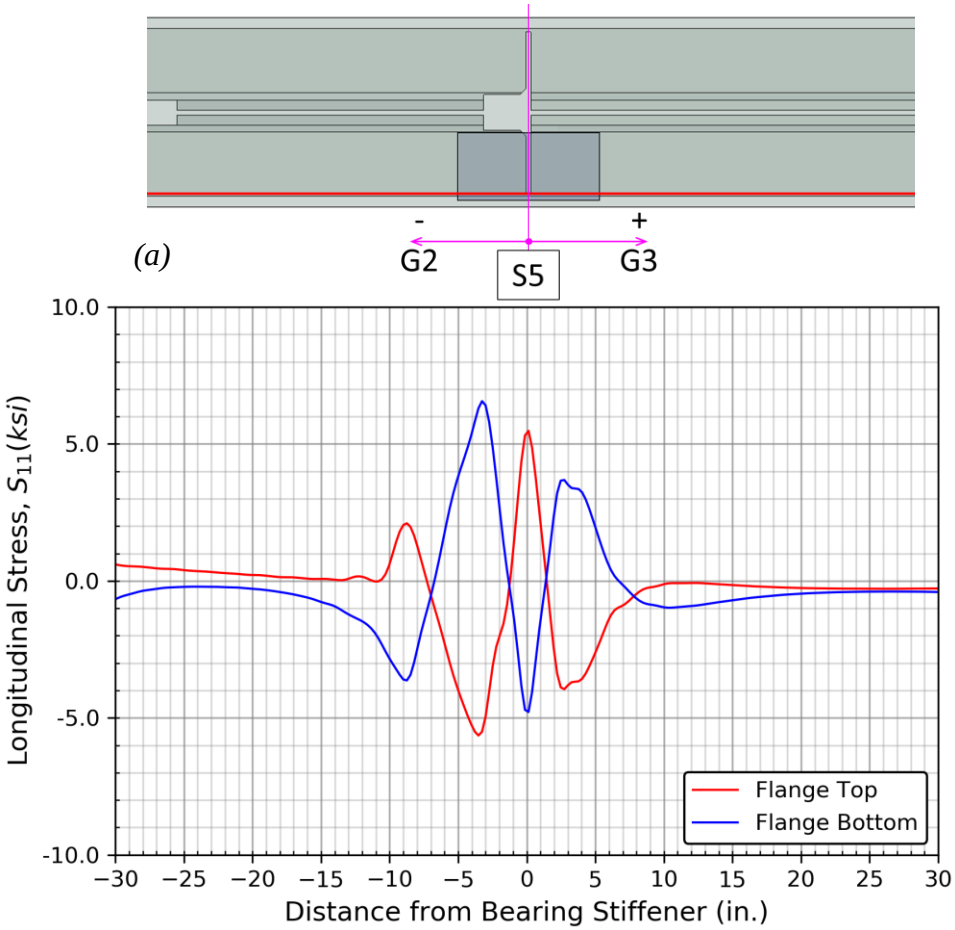

Figure 3-18 Longitudinal stress in the top flange of FB4 adjacent to S5 for load case L3T3: (a) plan view of top flange showing path and origin; (b) longitudianl stress along top and bottom paths

suggesting flexural deformation of the floor beam flange in the longitudinal direction under S5 bearing. The floor beam flange experienced reverse flexure, with negative moment (concave down deformation) over the bearing stiffener angle, rapidly changing to positive moment (convex up deformation) under the bearing footprint. The response was unsymmetric with respect to the bearing stiffeners, with the response to the west being slightly higher than the east. This is also evident from the contour plot of S_{11} presented in Figure 3-17. The maximum tensile stress on bottom of the connection angle leg, occurring at about 3.5 in. west of the bearing stiffener, was about 6.5 ksi. The maximum tensile stress at the top of the flange was about 5 ksi. Note that the bearing was $10\frac{1}{2}$ *in.* wide and the bearing retaining bolts were located 2 ½ *in.* from the centerline of the bearing stiffener. angle. The tensile stress in the flange at the bolt holes was about 4 ksi.

The variation of vertical stress (stress in the Y or 2-2 direction), S_{22} at the bearing stiffener-to-flange interface is presented in Figure 3-19 The stresses are determined on a path along the centerline of the protruding leg of the bearing stiffener angle. The plot is prepared with respect to the centerline of FB4 as origin. The distances are considered positive and negative respectively towards south and north, i.e., towards FB3 and FB5. The south bearing stiffener under the loaded S5 bearing experience compressive stress that increased almost linearly away from the centerline of the floor beam web. The north bearing stiffener was subjected to tensile stresses as the floor beam flange twisted due to the eccentric loading. The tensile stress increased up to about 4 in. from the centerline of the floor beam web and then decreased to almost zero. The maximum tensile stress was about 2 ksi.

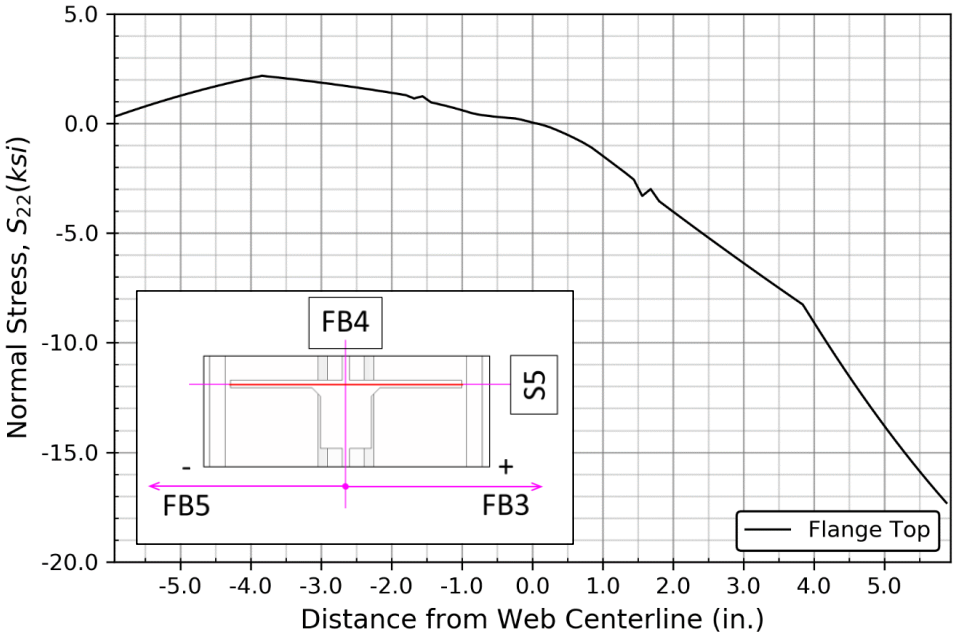

Figure 3-19 Vertical stress along path at soffit of FB4 top flange along centerline of bearing stiffener under S4 for load case L3T3

4 DISCUSSION OF RESULTS

The FEA results, presented in Section 3, showed that tensile live load stress as high as 75 ksi (assuming elastic behavior) occurred on the top of the upper flange of FB4 at the centerline of bearing stiffener for S4. Due to flexural response, a compressive stress as high as 68 ksi developed on the bottom of at the same location. These stresses occurred under the loaded bearing for the live load position, when the entire rear tandem axle of the notional fatigue truck moved over to one side of the deck expansion joint. Corresponding to this load case, there was practically no stress in the flange under the unload bearing on the other side of the deck expansion joint. Thus, the FB4 flange was expected to experience respectively 75 and 68 ksi tensile and compressive (elastic) stress range with the passage of the notional truck across the deck joint, resulting in local plastic strain cycling adjacent to the bearing stiffener in the flange angle. This large strain cycling is expected to cause fatigue cracking in the floor beam flange.

In the original construction, the bearing stiffeners at S4 were detailed as milled to bear. During the service life of the structure, however, some of the bearing stiffeners were repaired by welding plates to the stiffener and the flange angles to address section loss due to corrosion. Where the stiffeners were milled to bear, the flange angles developed fatigue cracking in the base meatal due to large strain cycles. At the weld-repaired details, fatigue cracking initiated at the weld toe and grew through the flange. Even though the weld toe was subjected to flexural compressive stresses, due to high tensile welding residual stress field at the compressive stress range resulted in a net tensile stress range. Considering that tensile welding residual stresses can be as high as the yield strength of the material, and assuming the angles to be of 36 ksi yield strength, the welded connection would experience a net tensile stress range of 36 ksi and fatigue crack growth.

The longitudinal tensile stress at the bottom surface of the flange adjacent to the holes for the bearing retaining bolts was about 20 ksi. Considering the stress concentration, the local stress range at the edge of the hole likely exceeded the yield stress of the material (36 ksi) and led to fatigue crack growth from the edge of the holes.

As presented in Figure 3-13, that bearing stiffener under S4 bearing experienced compressive bearing stress range of 22 ksi at the stiffener edge. When the stiffener was milled to bear, this stress range was well within the yield strength of the material (assumed 36 ksi) and was unlikely to contribute to fatigue crack growth. However, when the stiffener was welded to the floor beam flange, this compressive stress range in the presence of tensile welding residual stresses would effectively be tensile and could lead to fatigue crack growth through the stiffener-flange weld throat. Although this mode of cracking was not noted in the weld-repaired stiffener, since the demand for the crack growth from the weld toe into the flange (discussed in the previous paragraph) was more severe, branching of the crack parallel to the flange after initiating at the weld toe was noted. Fatigue racking through the throat of the stiffener-to-flange weld near the stiffener edge was noted for the bearing stiffener under S3 within the 1971 widened section with welded fabrication, where the stiffeners were welded to the flange.

Similar to the flange under S4, the floor beam flange under S5 experienced the maximum stress range as the rear tandem axle of the notional truck crossed over to one

side of the expansion joint. Compared to the floor beam flange under S4, however, the maximum longitudinal stress range in the floor beam flange under S5 of 5 ksi was significantly less. There are two reasons for this reduced response. First the depth of the variable depth floor beam under S4 is about 60 in., whereas the depth of the floor beam under S5 is about 72 in. Moreover, the knee brace to the floor beam exists at the centerline of S5, increasing the effective moment of inertia of the floor beam at the center line of S5. Second, the interior floor beam flange under S5 is built of two back-to-back 6×6×3/4 inch angles and a 14×5/8 in. cover plate, whereas the flange of the floor beam bracket under S4 is made of two back-to-back 6×4×1/2 angles, with the 6 in. leg forming the flange. The significant increase in the section modulus (and the flange area) would explain the reduction in stress range observed under S5.

The bearing stiffeners under S5 were fabricated as milled to bear. The stress range of 5 ksi at the bearing stiffener was insufficient to initiate any fatigue cracking adjacent to the stiffeners. The longitudinal tensile stress range on the bottom of the floor beam flange at the holes for the bearing retaining bolts was about 4 ksi. Conservatively assuming a stress concentration of 3.0, the local longitudinal stress range at the edge of the hole is estimated as 12 ksi, which was significantly less than 24 ksi, the AASHTO CAFT for base metal. Thus fatigue cracking in the flanges under S5 was unlikely. Indeed, no fatigue cracking has been reported at this location.

The maximum bearing stress range on the stiffener at S5 was about 18 ksi, which for a milled to bear connection is not likely to cause any fatigue cracking in the flange base metal.

5 CONCLUSIONS

5.1 Conclusions

Causes of unusual fatigue cracking of a steel bridge owned by the NJTA was investigated by advanced refined analysis using Finite Element Method. The bridge is located on a strategic commerce route and is subjected to large ADTT. The bridge originally built in 1950s and widened in 1971 is in service for more than 60 years. Fatigue cracking was observed in the top flange of the floor beams at deck expansion joints. The cracks developed at bearing stiffeners under the stringers and grew through the flange at some locations. A detailed 3D finite element model of part of the bridge including all features was developed and analyzed for site specific load. Based on WIM studies performed at a nearby bridge, the AASHTO HL93 fatigue design truck was found to be to the representative site specific loading. Significant presence of overloaded trucks having GVW as high as 160 kip was recorded in the truck traffic spectrum. Accordingly, the bridge model was analyzed for 2.25 times the AASHTO fatigue truck load plus 15% impact, generating 20.7 kip per wheel contact area of 10 × 20 in. Since the local response of the structure under wheel loads was of interest, the analysis was performed for the rear axle of the AASHTO fatigue truck, split into tandem configuration. The model was analyzed for three transvers and four longitudinal positions to simulate the moving load effects. All analyses were linear elastic.

The analysis results showed that the maximum stress in the floor beam flange developed when the rear tandem axle of the truck loading moved over to the deck on one side of the expansion joint. The maximum stress range developed under the loaded bearing on the floor beam bracket that was remnant from the original construction and was incorporated into the deck widening. At this location the flange was built with two angles without any cover plate. The longitudinal strains in the flange exceed the elastic limit of the material (assumed as 36 ksi). It was concluded that the fatigue cracking in the flange adjacent to the bearing stiffeners was due to cyclic plastic straining. The local stresses at the holes for the bearing retaining bolts also exceed the yield limit of the material that explained the fatigue cracks in the flange emanating from the holes. Due to significantly larger section modulus of the interior floor beam, the stresses in the flange was less than the AASHTO CAFT for Category A or base metal. No fatigue crack growth was observed nor was expected at this location.

The analysis showed that the fatigue cracking was due to larger ADTT and frequently occurring overloaded trucks in the truck traffic spectrum that exceeded the design fatigue limit state load in the AASHTO Specifications. The fatigue cracking was expected to be localized under the widened section of the bridge under the two exterior lanes mostly traversed by truck traffic, where the section modulus of the floor beam was lesser than that of the floor beams between the interior girders. Moreover, the interior floor beam was under interior lanes that is rarely traversed by truck traffic. This was also observed in the field.

5.2 Recommendations

Based on the findings it is recommended that the exterior floor beam between the exterior and the first interior girder be strengthened to reduce the stresses in the flange below the CAFT of respective details. The retrofit design should be optimized by additional stress analysis by finite element method, followed by limited laboratory and/or field studies. Additional analyses with increased refinement should also be performed to investigate the influence of the detailing adopted at the stringer bearings. In addition, the influence of changing the depth of the stringers for accommodating the elastomeric bearings should also be investigated.

5.3 Future Work

Future work should address the activities recommended above. The New Jersey Turnpike Authority has already agreed to pursue these tasks as a follow on to the research presented here. The researcher is communicating with NJTA and developing continued work. Given the importance of the structure on a strategic corridor, maintaining the bridge in a state of good repair is a must.

REFERENCES

1. Miner, M. A. (1945). “Cumulative damage in fatigue.” *Journal of Applied Mechanics.* 12: 149–164.
2. Fisher, J.W., Nussbaumer, A., Keating, P.B., and Yen, B.T. (1993). Resistance of Welded Details Under Variable Amplitude Long-Life Fatigue Loading. *NCHRP Report 354*. Transportation Research Board, Washington D.C.